Title

Flow-Responsive Vascular Endothelial Growth Factor Receptor-Protein Kinase C Isoform Epsilon Signaling Mediates Glycolytic Metabolites for Vascular Repair.

Journal

Antioxidants & redox signaling, 28(1)

ISSN

1523-0864

Authors

Baek, Kyung In
Li, Rongsong
Jen, Nelson
et al.

Publication Date

2018

DOI

10.1089/ars.2017.7044

Peer reviewed

ANTIOXIDANTS & REDOX SIGNALING
Volume 28, Number 1, 2018

DOI: 10.1089/ars.2017.7044

Discoveries

ORIGINAL RESEARCH COMMUNICATION

Flow-Responsive Vascular Endothelial Growth Factor Receptor-Protein Kinase C Isoform Epsilon Signaling Mediates Glycolytic Metabolites for Vascular Repair

Kyung In Baek,[1] Rongsong Li,[2] Nelson Jen,[1] Howard Choi,[2] Amir Kaboodrangi,[1] Peipei Ping,[2,3] David Liem,[2] Tyler Beebe,[1] and Tzung K. Hsiai[1–5]

Abstract

Aims: Hemodynamic shear stress participates in maintaining vascular redox status. Elucidating flow-mediated endothelial metabolites enables us to discover metabolic biomarkers and therapeutic targets. We posited that flow-responsive vascular endothelial growth factor receptor (VEGFR)-protein kinase C isoform epsilon (PKCε)-6-phosphofructo-2-kinase/fructose-2,6-biphosphatase 3 (PFKFB3) signaling modulates glycolytic metabolites for vascular repair.

Results: Bidirectional oscillatory flow (oscillatory shear stress [OSS]: 0.1 ± 3 dyne·cm^{-2} at 1 Hz) upregulated VEGFR-dependent PKCε expression to a greater degree than did unidirectional pulsatile flow (pulsatile shear stress [PSS]: 23 ± 8 dyne·cm^{-2} at 1 Hz) in human aortic endothelial cells ($p < 0.05$, $n = 3$). PSS and OSS further upregulated PKCε-dependent PFKFB3 expression for glycolysis ($p < 0.05$, $n = 4$). Constitutively active PKCε increased, whereas dominant-negative PKCε reduced both basal and maximal extracellular acidification rates for glycolytic flux ($p < 0.01$, $n = 4$). Metabolomic analysis demonstrated an increase in PKCε-dependent glycolytic metabolite, dihydroxyacetone (DHA), but a decrease in gluconeogenic metabolite, aspartic acid ($p < 0.05$ *vs.* control, $n = 6$). In a New Zealand White rabbit model, both PKCε and PFKFB3 immunostaining was prominent in the PSS- and OSS-exposed aortic arch and descending aorta. In a transgenic *Tg(flk-1:EGFP)* zebrafish model, *GATA-1a* morpholino oligonucleotide injection (to reduce viscosity-dependent shear stress) impaired vascular regeneration after tail amputation ($p < 0.01$, $n = 20$), which was restored with PKCε messenger RNA (mRNA) rescue ($p < 0.05$, $n = 5$). As a corollary, siPKCε inhibited tube formation and vascular repair, which were restored by DHA treatment in our Matrigel and zebrafish models.

Innovation and Conclusion: Flow-sensitive VEGFR-PKCε-PFKFB3 signaling increases the glycolytic metabolite, dihydroxyacetone, to promote vascular repair. *Antioxid. Redox Signal.* 28, 31–43.

Keywords: shear stress, metabolites, PKCε, PFKFB3, dihydroxyacetone, vascular repair

Introduction

HEMODYNAMIC FORCES MODULATE mammalian cell metabolism (19). Unidirectional pulsatile and bi-directional oscillatory flow largely determine the focal but eccentric distribution of vascular oxidative stress (8, 22, 38), post-translational protein modifications, and metabolic pathways (17, 19, 22). Metabolomic analyses have led to the discovery of new metabolic biomarkers and therapeutic targets, including polyamines such as spermine for acute stroke, cinnamoylglycine, nicotinamide, and cysteine-glutathione disulfide for renal cancer, and 3-hydroxykynurenine and oxidized glutathione for Parkinson disease (1, 2, 10). Thus, elucidation of flow-mediated metabolomic changes provides an entry point to

[1]Department of Bioengineering, School of Engineering and Applied Science, University of California, Los Angeles, Los Angeles, California.
[2]Division of Cardiology, Department of Medicine, University of California, Los Angeles, Los Angeles, California.
[3]Department of Physiology, School of Medicine, University of California, Los Angeles, Los Angeles, California.
[4]Greater Los Angeles VA Healthcare System, Los Angeles, California.
[5]Department of Medical Engineering, California Institute of Technology, Pasadena, California.

Innovation

Hemodynamic shear stress participates in epigenomic changes to maintain endothelial homeostasis. We uncovered a vascular metabolite, dihydroxyacetone, for vascular repair *via* flow-responsive vascular endothelial growth factor (VEGF) receptor-protein kinase C isoform epsilon (PKCε)-6-phosphofructo-2-kinase/fructose-2,6-biphosphatase 3 (PFKFB3) signaling, thus providing a novel mechano-metabolomic pathway for vascular repair.

uncover metabolites participating in endothelial homeostasis (27, 51), migration (56), vascular development (12), and physical activity (39).

Pulsatile shear stress (PSS) and oscillatory shear stress (OSS) differentially activate canonical Wnt-β-catenin signaling to modulate vascular development and repair (14, 33). PSS and OSS promote the differentiation of embryonic stem cells to vascular progenitors in angiogenesis (5, 45). Laminar flow-dependent vascular endothelial growth factor (VEGF) and endothelial nitric oxide synthase (eNOS) phosphorylation induce nitric oxide (•NO)-mediated protein kinase C isoform epsilon (PKCε) signaling to confer mitochondrial homeostasis (4, 55). Although VEGF-mediated angiogenesis promotes tumor initiation and progression (3, 43), the mechanisms underlying flow-mediated VEGF-PKCε signaling to modulate endothelial metabolites for vascular repair remain unexplored.

Endothelial glycolysis is mechano-responsive (49). Glucose uptake in endothelial cells (ECs) is metabolized to pyruvate *via* the glycolytic pathway (11). Rather than relying on oxidative metabolism for mitochondrial respiration, ECs generate more than 80% of their ATP from the glycolytic pathway (11). ECs increase their glycolytic flux when switching from quiescence to proliferation and migration states (13). A recent study reports that laminar shear stress (LSS) activates Krüppel-like factor 2 (KLF2) to suppress 6-phosphofructo-2-kinase/fructose-2,6-biphosphatase 3 (PFKFB3)-mediated glycolysis in ECs, mitigating angiogenesis and vessel sprouting (15), whereas flow-sensitive VEGF receptor (VEGFR) signaling upregulates PFKFB3-driven glycolysis (12, 13). Shear-mediated nitric oxide production induces PKCε (25, 54), which, in turn, attenuates mitochondrial reactive oxygen species (ROS) after ischemia/reperfusion (I/R) injury (6, 36). Flow-responsive VEGF-eNOS signaling activates PKCε to modulate EC proliferation, lumen formation, and homeostasis (28, 44). Nevertheless, the mechanotransduction mechanism underlying PKCε-mediated metabolomic pathways to mediate vascular repair remains elusive.

In this context, we sought to elucidate the flow-sensitive VEGFR-PKCε signaling to mediate glycolytic metabolites for vascular repair. Both PSS and OSS promoted VEGFR-dependent PKCε and PFKFB3 expression to promote glycolytic flux. Further, we demonstrated that shear stress-mediated PKCε signaling rescued vascular regeneration in *Tg(flk-1:EGFP)* zebrafish tail amputation model, and the glycolytic metabolite, dihydroxyacetone (DHA), restored tube formation and vascular repair in response to silencing PKCε. Thus, our study indicates that flow-sensitive VEGFR-PKCε signaling promotes glycolytic metabolites for vascular repair.

Results

Flow-responsive PKCε mediated endothelial glycolysis

PSS and OSS differentially increased PKCε messenger RNA (mRNA) expression by 65% and 134%, respectively, whereas the VEGFR inhibitor, cediranib at 10 μM or VEGFR2 knockdown with small interfering RNA (siRNA) inhibited shear stress-induced PKCε mRNA and protein expression (Fig. 1A and Supplementary Fig. S1A; Supplementary Data are available online at www.liebertpub.com/ars). PSS and OSS further increased PKCε activity by 60% and 65%, respectively (Fig. 1B). PSS and OSS also increased PFKFB3 mRNA and protein expression, which was attenuated by siPKCε (Fig. 1C and Supplementary Fig. S1C). As a corollary, constitutively active PKCε (CA-PKCε) *via* recombinant adenovirus (Adv-CA-PKCε) infection increased, whereas dominant-negative PKCε (DN-PKCε) decreased PFKFB3 mRNA and protein expression ($p < 0.05$ *vs.* Adv-LacZ control, $n = 3$) (Fig. 1D and Supplementary Fig. S1B). PKCε and PFKFB3 immunostaining was present in PSS- and OSS-exposed endothelial lining in the aortic arch and thoracic aorta from the New Zealand White (NZW) rabbits (Supplementary Fig. S2).

In addition, PKCε-mediated metabolic activity was quantified by using a SeaHorse Flux Analyzer. CA-PKCε increased basal (3.11-fold, $p < 0.01$, $n = 4$) and maximum extracellular acidification rates (ECAR; 2.52-fold, $p < 0.01$ *vs.* DN-PKCε, $n = 4$) for proton production as an indicator of glycolytic flux (57). This elevated glycolytic flux was further validated with H_2O_2 (50 μM)-induced oxidative stress (2.13-fold basal ECAR, 2.45-fold maximum ECAR, $p < 0.01$, $n = 4$) (Fig. 1E, F).

Shear stress modulated PKCε-dependent glycolytic metabolites

Our metabolomic analysis of 156 human aortic endothelial cells (HAEC) metabolites with a known identity (Supplementary Table S1) revealed that 4 metabolites were significantly upregulated in response to PSS and OSS, including putrescine ($C_4H_{12}N_2$) and dihydroxyacetone ($C_3H_6O_3$), whereas aspartic acid ($C_4H_7NO_4$) was decreased (Supplementary Fig. S3). To validate flow-mediated glycolytic metabolites, we performed metabolomic analysis in HAEC transfected with scrambled (Scr) siRNA or siPKCε in response to (i) static, (ii) PSS, and (iii) OSS conditions. Principal component analysis (PCA) demonstrated significant separation among 16 metabolites in the scrambled (Scr) group and among 13 in the siPKCε group ($p < 0.05$, $n = 6$) (Fig. 2A–D). Both PSS and OSS upregulated putrescine, glucose ($C_6H_{12}O_6$), fructose ($C_6H_{12}O_6$), and DHA. In the presence of siPKCε transfection, OSS attenuated glucose, fructose, and DHA to a greater degree than did PSS. siPKCε transfection also increased glucose and fructose, implicating a reduction in glycolysis and/or fructolysis. Further, siPKCε attenuated both PSS- and OSS-mediated increases in DHA (Fig. 2E). Thus, both PSS and OSS modulated PKCε-dependent glucose, fructose, and DHA as well as PKCε-independent putrescine.

PKCε mediated tube formation and vascular repair

In an *in vitro* Matrigel model, siPKCε decreased endothelial tube formation by 40% as quantified by tube lengths ($p < 0.05$ *vs.* Scr siRNA, $n = 3$) (Fig. 3A, B). CA-PKCε

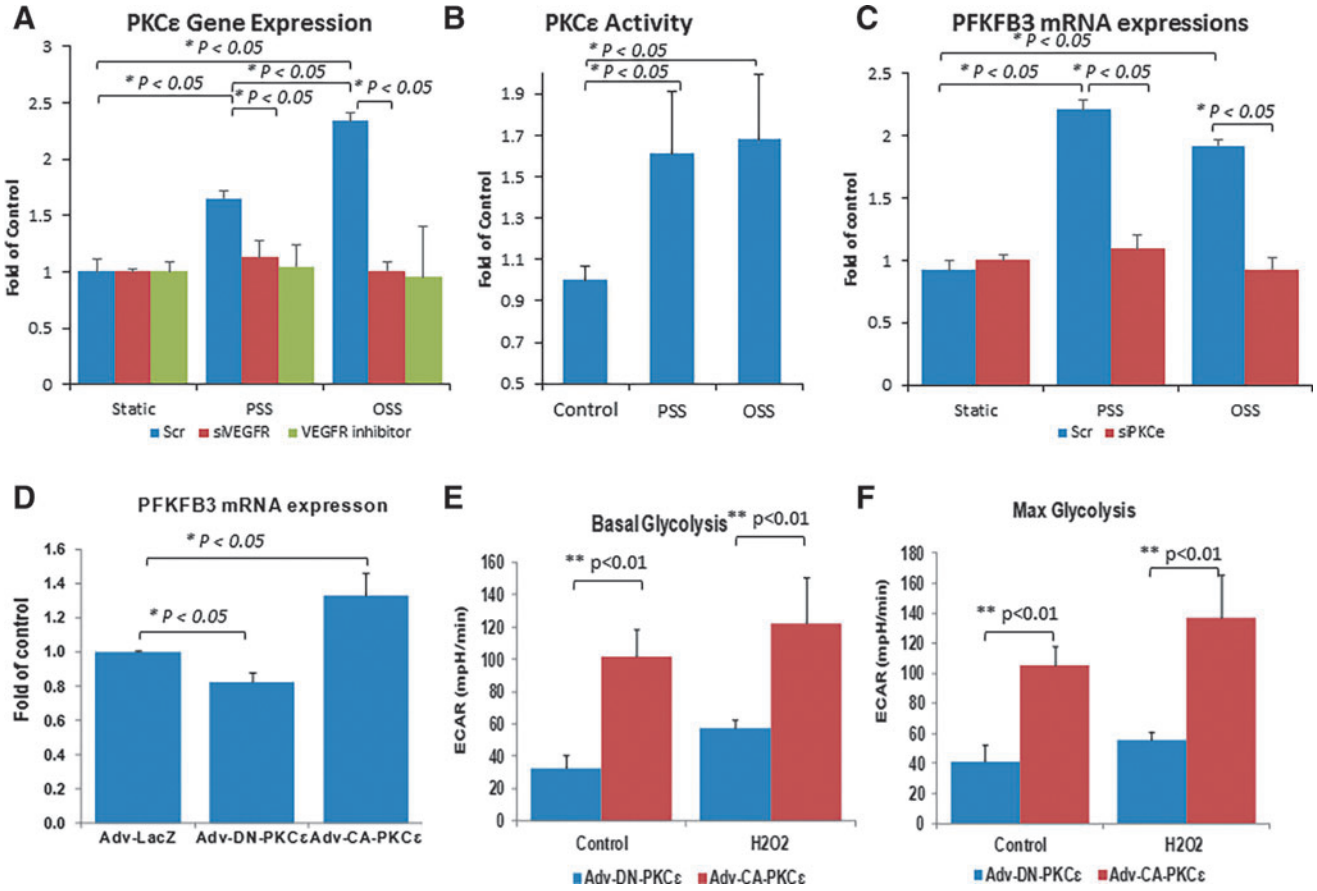

FIG. 1. Shear stress-responsive VEGFR-PKCε-PFKFB3 signaling. (A) HAEC were transfected with scrambled (Scr) siRNA or VEGFR2 siRNA (siVEGFR2), or they were treated with or without VEGFR inhibitor. PSS and OSS differentially upregulated VEGFR2-dependent PKCε mRNA expression ($*p<0.05$, $n=3$). **(B)** PSS and OSS further upregulated PKCε activity ($*p<0.05$, $n=3$). **(C)** PSS and OSS also upregulated PFKFB3 mRNA expression, which was abrogated in response to siPKCε ($*p<0.05$, $n=4$). **(D)** CA-PKCε promoted, whereas DN-PKCε reduced the PFKFB3 mRNA expression ($*p<0.05$ *vs.* LacZ control, $n=3$). **(E, F)** Seahorse assay revealed that CA-PKCε increased both **(E)** basal and **(F)** max ECAR at the baseline and in response to H_2O_2 at 50 μM ($*p<0.01$ *vs.* DN-PKCε, $n=4$). CA, constitutively active; DN, dominant negative; ECAR, extracellular acidification rates; HAEC, human aortic endothelial cells; mRNA, messenger RNA; OSS, oscillatory shear stress; PFKFB3, 6-phosphofructo-2-kinase/fructose-2,6-biphosphatase 3; PKCε, protein kinase C isoform epsilon; PSS, pulsatile shear stress; siRNA, small interfering RNA; VEGFR, vascular endothelial growth factor receptor. To see this illustration in color, the reader is referred to the web version of this article at www.liebertpub.com/ars

increased tube formation by 2.1-fold ($p<0.05$ *vs.* LacZ, $n=3$) (Fig. 3C, D). VEGFR inhibitor, cediranib, disrupted tube formation in Adv-LacZ-infected HAEC (Fig. 3C, D), and this disruption was restored with Adv-CA-PKCε (Fig. 3C, D). Glycolysis-relevant metabolites (glucose, fructose, and DHA) promoted HAEC tube formation, whereas a gluconeogenesis-relevant metabolite (aspartic acid) had no effects (Supplementary Fig. S4).

In a transgenic *Tg(flk-1:EGFP)* zebrafish model of tail regeneration, control *p53* morpholino oligonucleotide (MO) injection supported vascular regeneration as visualized by a closed loop between the dorsal longitudinal anastomotic vessels and dorsal aortas at 3 days post-amputation (dpa) (Fig. 3E). *PKC*ε MO injection impaired, whereas *PKC*ε mRNA restored vascular regeneration at 3 dpa (Fig. 3E). Taken together, PKCε-mediated glycolytic metabolites promoted tube formation and vascular repair.

Genetic manipulations of shear stress-mediated vascular repair

After *GATA-1a* MO injection to reduce viscosity-dependent shear stress (Supplementary Videos S1 and S3), zebrafish embryos failed to develop vascular regeneration at 3 dpa until 5 dpa ($p<0.05$ *vs.* control, $n=30$) (Fig. 4C). After *TNNT-2* MO injection to inhibit myocardial contraction and blood flow, zebrafish embryos also failed to develop tail regeneration at 3 dpa ($p<0.05$ *vs.* control, $n=5$) (Fig. 4E), and they failed to thrive at 5 dpa. After erythropoietin mRNA injection to augment erythrocytosis as a means of restoring viscosity-dependent shear stress (Supplementary Video S2), zebrafish embryos developed tail regeneration at 3 and 5 dpa ($p<0.05$ *vs.* control, $n=30$) (Fig. 4E). As a corollary, rescue of *GATA-1a* MO-injected embryos with *PKC*ε mRNA restored vascular regeneration at 3 and 5 dpa ($p<0.05$

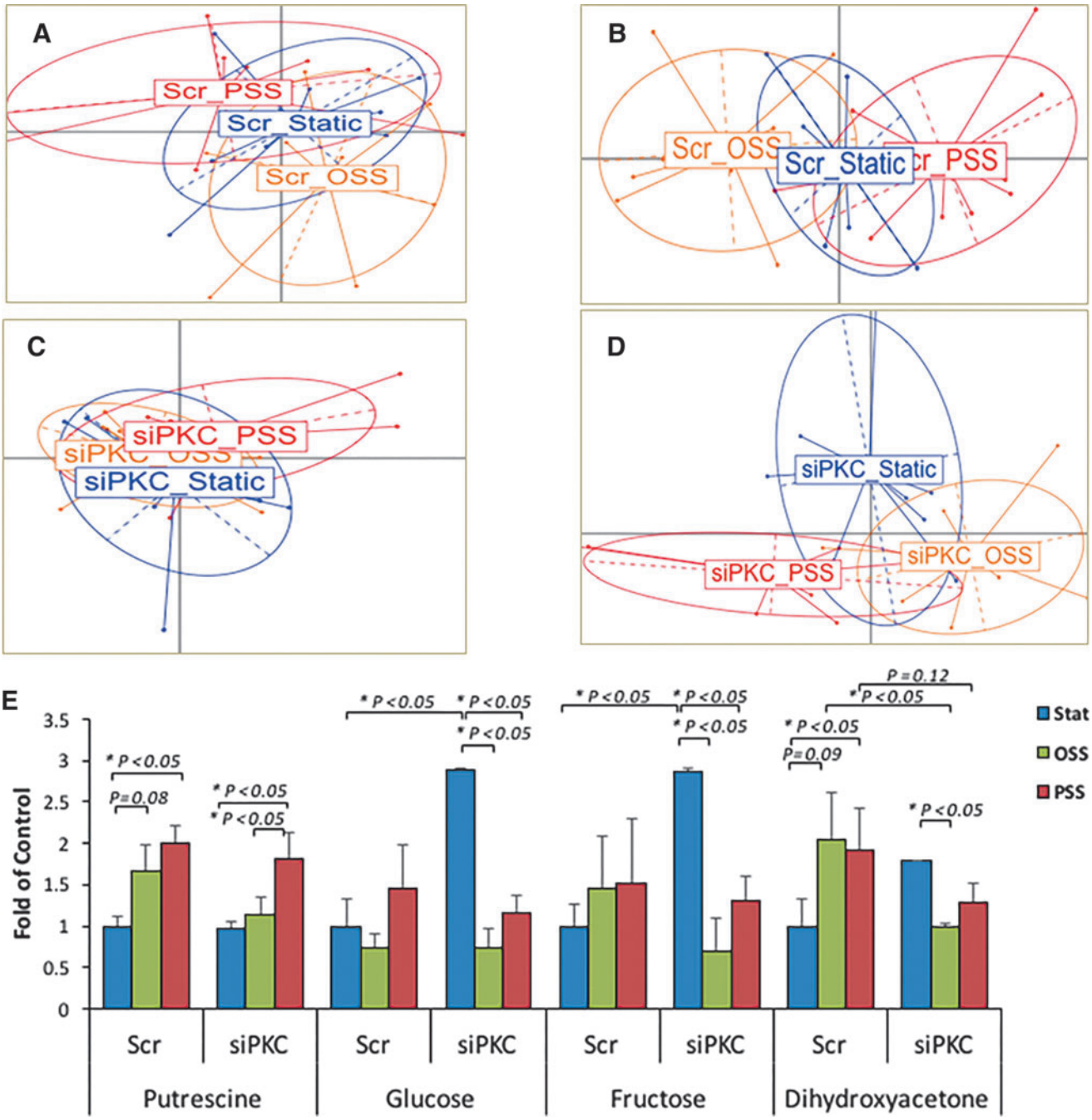

FIG. 2. Shear stress-mediated PKCε-dependent metabolites. HAEC were transfected with scramble (Scr) siRNA or PKCε siRNA (siPKC), followed by three conditions: (i) static state, (ii) PSS, or (iii) OSS for 4 h. **(A, C)** Of the 136 known metabolites, PCA revealed significant overlapping of metabolites after the static, OSS, and PSS conditions in both Scr and siPKCε-transfected HAEC. **(B, D)** The concentration of 16 metabolites in Scr and 13 in siPKCε groups was significantly changed after the three conditions ($*p < 0.05$, $n = 6$). PCA revealed a separation among the statistically different metabolites. **(E)** PSS and OSS significantly modulated the selected metabolites, demonstrating PKCε-dependent Glucose, Frucose, DHA, and PKCε-independent Putrescine ($*p < 0.05$, $n = 6$). DHA, dihydroxyacetone; PCA, principal component analysis. To see this illustration in color, the reader is referred to the web version of this article at www.liebertpub.com/ars

vs. GATA-1a MO-alone injected group, $n = 30$) (Fig. 4F). Vascular repair was quantitatively compared in response to the genetic manipulations (Fig. 4G), supporting the important roles of shear stress and PKCε to promote vascular repair.

PKCε-dependent DHA rescued vascular repair

In an *in vitro* Matrigel model, siPKCε attenuated tube formation, which was partially rescued by the PKCε-dependent glycolytic metabolite, DHA ($p < 0.05$ *vs.* Scr siRNA, $n = 4$)

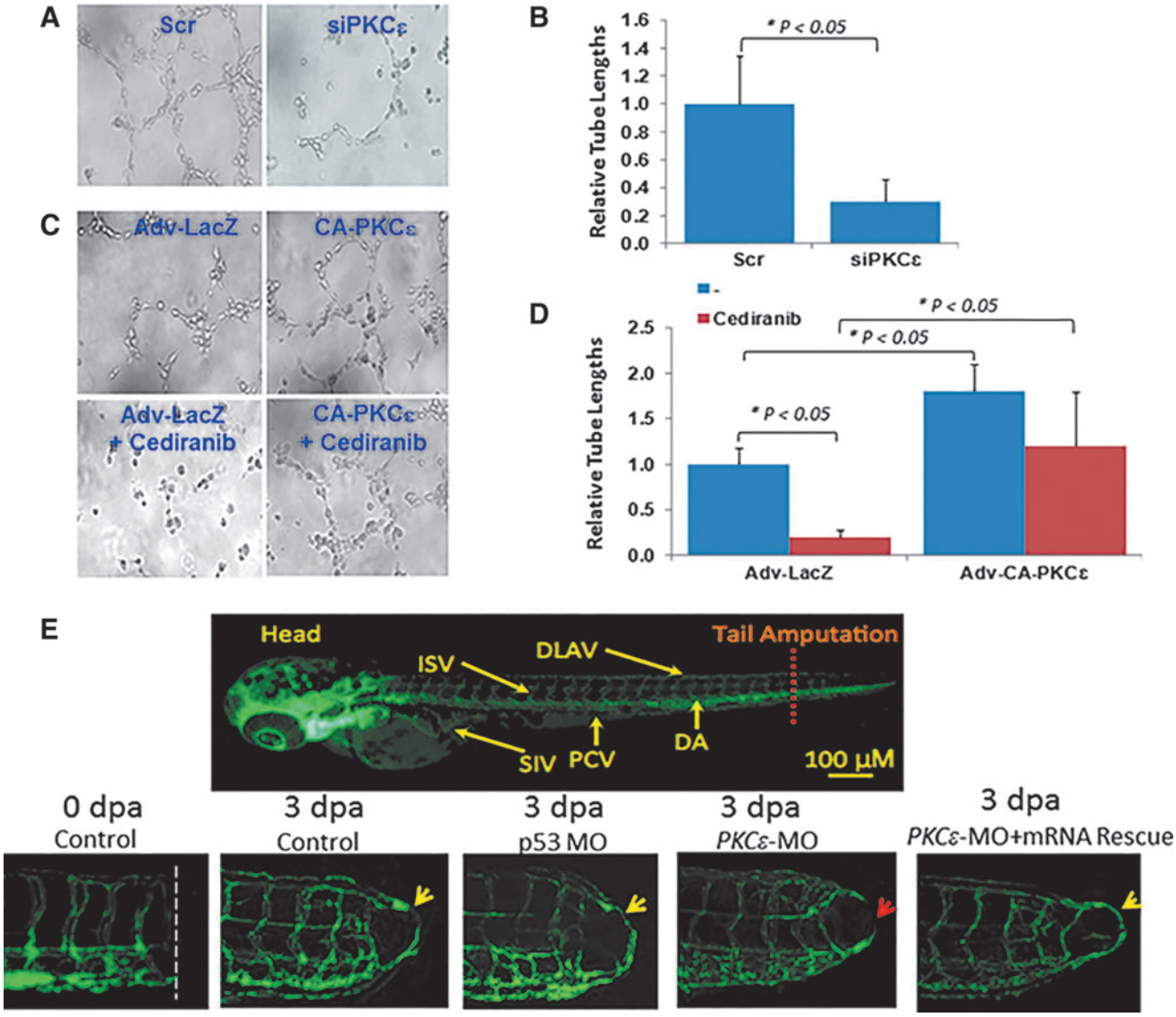

FIG. 3. PKCε-mediated tube formation and vascular repair. (A) HAEC were transfected with scrambled (Scr) siRNA or PKCε siRNA (siPKCε). **(B)** siRNA attenuated tube formation, which was quantified by the changes in tube lengths. **(C, D)** HAEC were infected with recombinant control LacZ or CA-PKCε adenoviruses. Treatment with Cediranib at 10 μM inhibited tube formation ($^*p < 0.05$, $n = 5$), whereas CA-PKCε restored Cediranib-attenuated tube formation ($^*p < 0.05$, $n = 5$). **(E)** Transgenic *Tg(flk-1:EGFP)* embryos underwent tail amputation as a mode of vascular regeneration. The control group and *p53* MO-injected embryos exhibited vascular repair (*yellow arrows*) by re-connecting DLAV with DA. *PKC*ε MO injection impaired vascular repair (*red arrow*), whereas co-injecting *PKC*ε mRNA restored vascular repair (*yellow arrow*). DA, dorsal aorta; DLAV, dorsal longitudinal anastomotic vessel; ISV, intersegmental vessel; MO, morpholino oligonucleotide; PCV, posterior cardinal vein; SIV, subintestinal vessel. To see this illustration in color, the reader is referred to the web version of this article at www.liebertpub.com/ars

(Fig. 5A, B). In the zebrafish tail amputation model, DHA restored vascular repair from 67% to 100% in the control MO-injected fish at 6 dpa ($p < 0.05$ *vs.* control, $n = 4$). Further, DHA rescued vascular repair from 30% to 80% in PKCε MO-injected fish ($p < 0.05$ *vs.* control, $n = 30$) (Fig. 5C, D). These findings strengthen the notion that PKCε-dependent DHA promoted endothelial tube formation and vascular repair.

Discussion

The novelty of this study resides in establishing flow-mediated VEGFR-PKCε-PFKFB3 signaling to promote glycolytic metabolite, DHA, for vascular repair. Metabolomic analysis revealed that PSS and OSS modulated PKCε-dependent endothelial PFKFB3 expression to mediate glycolytic metabolites. In the NZW rabbit aortic arch and descending aorta, PKCε and PFKFB3 immunostaining was present in the PSS- and OSS-exposed regions. In the zebrafish model of tail amputation, shear stress plays an important epigenetic role with PKCε to mediate vascular regeneration. Thus, we provide a new mechano-metabolomic pathway to increase the glycolytic metabolite, DHA, for vascular regeneration (Fig. 6).

Our data support that the characteristics of flow, namely PSS ($\tau_{ave} = 50$ dyne$\cdot$cm^{-2} accompanied by a slew rate at $\partial\tau$/

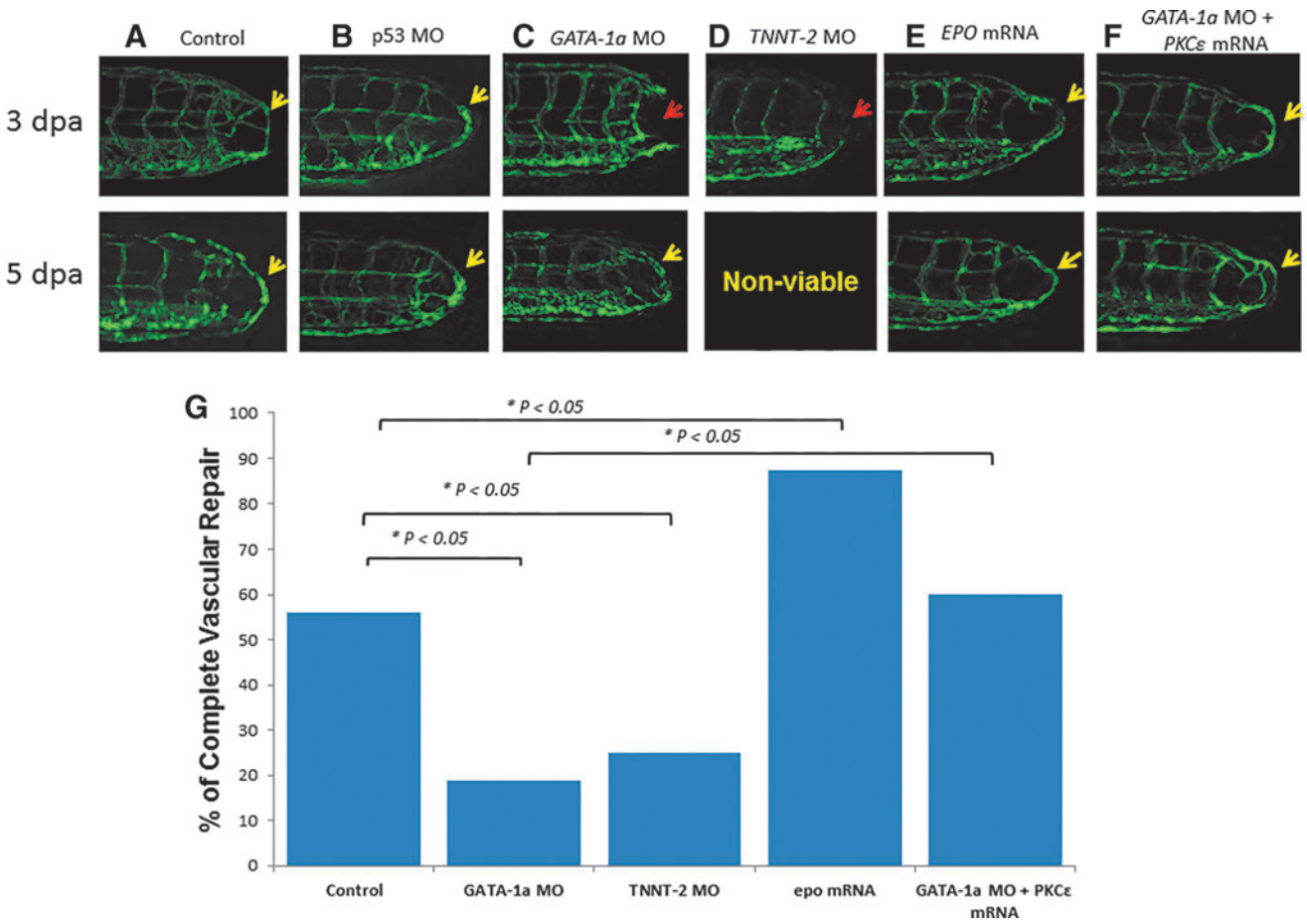

FIG. 4. Shear stress-mediated vascular repair. (A, B) The control and *p53* MO-injected fish developed vascular repair at 3 dpa (*yellow arrows*). **(C)** *GATA-1a* MO delayed vascular repair at 3 dpa. **(D)** *TNNT-2* MO impaired vascular repair (*red arrow*) at 3 dpa ($*p < 0.05$, $n = 5$), and the embryos failed to thrive at 5 dpa. **(E)** *EPO* mRNA injection promoted vascular repair at 3 dpa. (**F**) Co-injection of *GATA-1a* MO with *PKC*ε mRNA resulted in vascular repair. **(G)** Quantitative comparison revealed differential percentage of vascular repair ($*p < 0.05$, $n = 30$; $n = 5$ for *TNNT-2* MO injected group). dpa, days post-amputation; EPO, erythropoietin. To see this illustration in color, the reader is referred to the web version of this article at www.liebertpub.com/ars

$\partial t = 71$ dyne·cm^{-2}·s^{-1} at 1 Hz) and OSS (0 ± 3 dyne·cm^{-2} with $\tau_{ave} = 0$ dyne·cm^{-2} at 1 Hz), modulate VEGFR-PKCε-PFKFB3 signaling to increase glycolytic metabolites (Fig. 1E). Doddaballapur *et al.* reported that LSS ($\tau_{ave} = 20$ dyne·cm^{-2} at steady state, $\partial\tau/\partial t = 0$) reduced KLF2-dependent PFKFB3 promoter activity to reduce glycolysis (15), leading to attenuation in angiogenic sprouting (13, 46). However, the differential effects of LSS *versus* OSS to modulate AMPK and Akt activities are well recognized to promote glycolysis (21). Further, Jalali *et al.* demonstrated the role of p60scr and RAS in shear stress-activated endothelial MAPK signaling (23), whereas induction of PFKFB3 expression in response to MAPK activation has been previously reported in cancer cells (40). Taken together, these observations highlight the differential characteristics of shear stress to mediate PFKFB3 expression (22, 34).

Hemodynamic shear forces modulate vascular metabolism to maintain cellular homeostasis (27, 51). Our metabolomic analyses *via* gas chromatography time-of-flight mass spectrometry (GC-TOF) revealed that PSS and OSS increased DHA, fructose, glucose, and putrescine (Fig. 2). DHA is an intermediate metabolite of fructose metabolism, participating in glycolysis in its phosphate form (42). As a corollary, the glycolysis-related metabolites (namely alanine, glucose, and lactate) were also elevated in response to I/R in the CA-PKCε mouse (36). Thus, these glycolytic metabolites provide a basis for cellular homeostasis (27, 51) and migration (56), vascular development (12), and physical activity (39).

PFKFB3 is a key regulator of glycolysis to promote angiogenic sprouting (12). In response to the transition from quiescence to proliferation and migration, vascular ECs developed an increased glycolytic flux (13). During migration, glycolytic enzymes are translocated to lamellipodia for ATP production (13). Inhibition of PFKFB3 decreases stalk cell proliferation and tip cell migration (12) to reduce vessel sprouting (46). We further demonstrated PKCε-dependent PFKFB3 expression (Fig. 1C, D) and prominent PKCε and PFKFB3 immunostaining in the shear-exposed NZW aorta (Supplementary Fig. S2), supporting the notion that flow-mediated VEGFR-PKCε-PFKFB3 signaling promotes vascular regeneration.

PKC isoforms are distributed in numerous tissues and cell types. Three phorbol ester/diacylglycerol-dependent PKC isoforms, α-, δ-, and ε-, are highly expressed in the myocardium (26). PKCδ and PKCε are two Ca^{2+}-independent

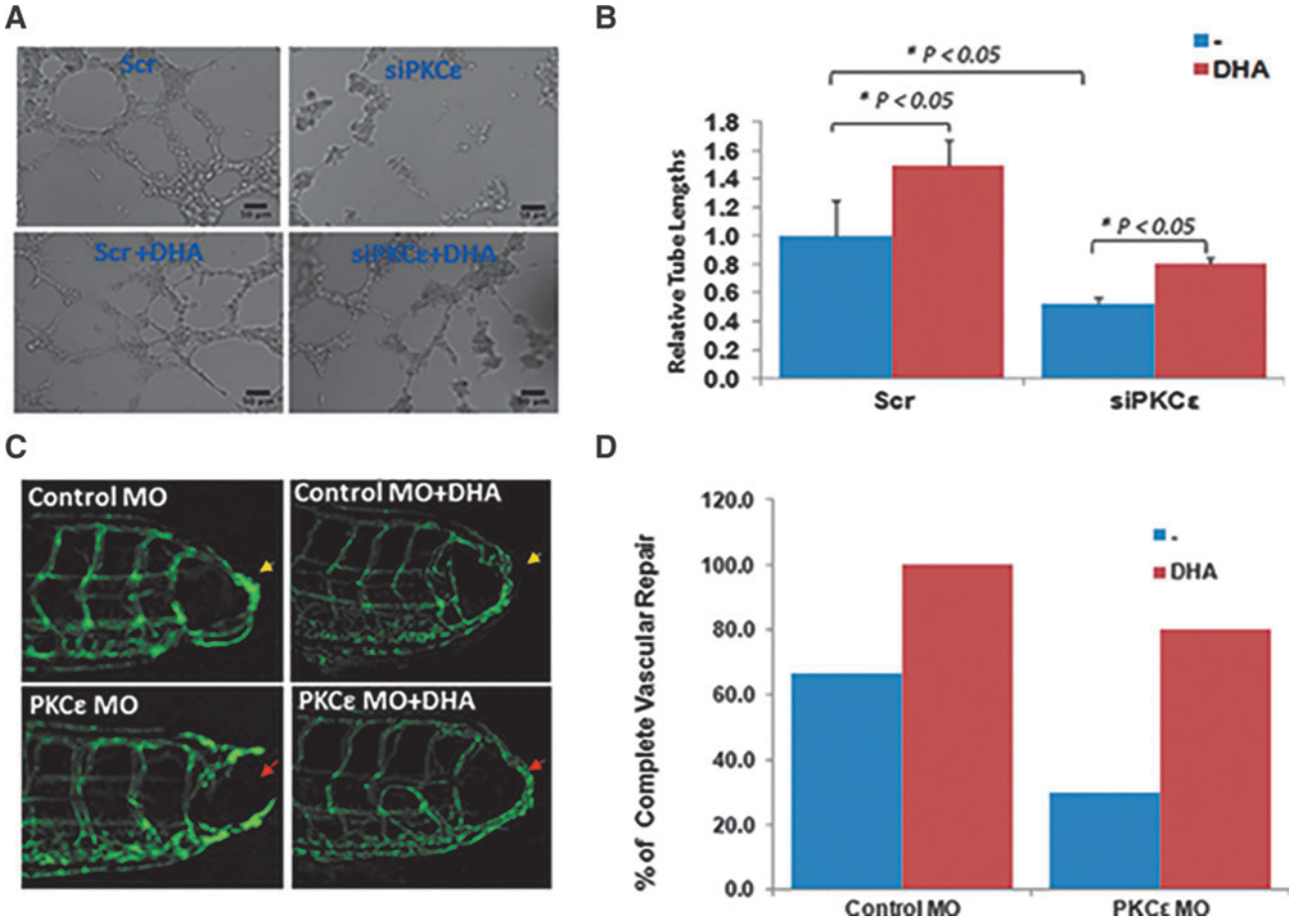

FIG. 5. Glycolytic metabolite DHA promoted vascular repair. (A–B) DHA promoted tube formation in HAEC transfected with scrambled (Scr) siRNA. siPKCε attenuated tube formation, which was rescued with DHA at 1 mg/ml (*$p < 0.05$, $n = 4$). **(B)** Provides quantifications of the relative tube length for **(A)**. **(C)** *Tg (flk-1:EGFP)* embryos injected with *p53* MO or *PKC*ε MO underwent tail amputation, and they were treated with or without DHA (1 mg/ml) for 3 days. DHA treatment rescued impaired vascular repair after *PKC*ε MO injection. **(D)** Vascular repair was quantified by the percentage of embryos that developed vascular regeneration ($n = 20$). To see this illustration in color, the reader is referred to the web version of this article at www.liebertpub.com/ars

isoforms implicated in regulation of growth, differentiation, and apoptosis of ventricular cells (16). PKCε over-expression in the CA-PKCε mouse increased glycolytic metabolites in association with cardioprotection after I/R injury (36). CA-PKCε over-expression further attenuated H_2O_2-mediated endothelial mitochondrial super oxide ($O_2^{\bullet-}$) production (Supplementary Fig. S5). In addition to increasing glycolytic flux (Supplementary Fig. S2E), CA-PKCε reduced p62 protein level to promote autophagic flux (Supplementary Fig. S6B). In this context, we present evidence of flow-mediated PKCε signaling to modulate endothelial homeostasis for tube formation and vascular repair.

Zebrafish (*Danio rerio*) comprise a well-established genetic system for studying cardiovascular development and disease (30, 37, 47). Use of zebrafish allows for genetic manipulations of viscosity to change shear stress (Fig. 4) [Eq. (1)]. Injection of *GATA*-1a MO significantly inhibits erythropoiesis up to 6 days post-fertilization (29), resulting in a reduction in viscosity to decrease shear stress, whereas an injection of erythropoietin (*EPO*) mRNA promotes erythrocytosis (9), resulting in a rise in viscosity to increase shear stress. Thus, use of the zebrafish system enabled us to recapitulate shear stress-mediated vascular repair *via* PKCε and glycolytic metabolite, DHA.

The NZW rabbits are a well-established atherosclerotic model for interrogation of the metabolically active lesions (35, 41). Similar to humans, NZW rabbits developed oxidized low-density lipoprotein-rich lesions in response to high-fat-induced hypercholesterolemia (7, 24, 58), thereby providing an *ex vivo* model to validate endothelial PKCε and PFKFB3 expression (Supplementary Fig. S2). In this context, both *in vivo* zebrafish and *ex vivo* NZW rabbit models are complementary and synergistic to strengthen the vascular endothelial phenotypes (31).

Despite differential PKCε mRNA and protein expression in response to PSS and OSS (Fig. 1A), we observed similar levels of PKCε activity. PKCε is activated by phosphorylation (Fig. 1B), and this non-linear relation may stem from post-translational modifications of PKCε protein to influence the level of PKCε phosphorylation (Fig. 1B), and subsequent PFKFB3 mRNA expression. In addition, the PSS- and OSS-responsive NADPH oxidase system generates ROS (22, 34).

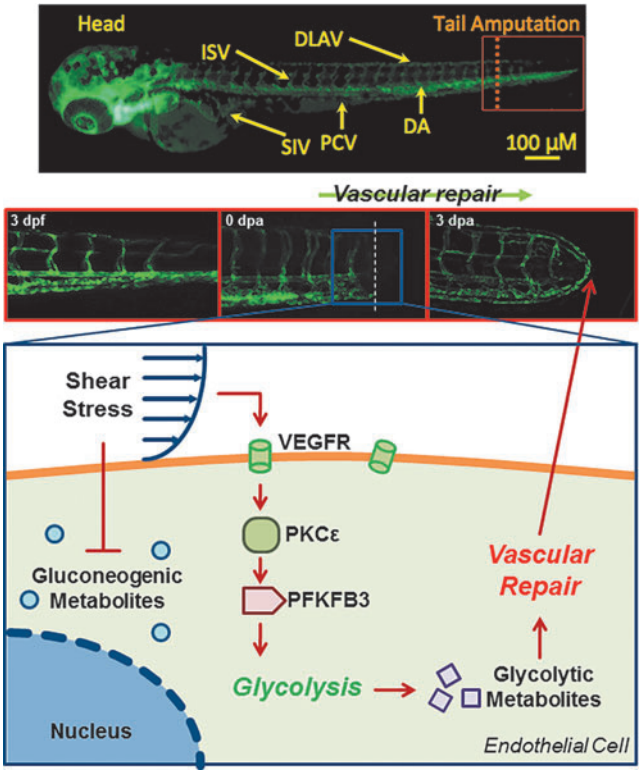

FIG. 6. A schematic diagram depicts flow-sensitive VEGFR-PKCε-PFKFB3 modulation of glycolytic metabolites for vascular repair. To see this illustration in color, the reader is referred to the web version of this article at www.liebertpub.com/ars

Despite an increase in PKCε protein expression (Fig. 1A), the concomitant production in ROS may be implicated in ubiquitination and protein degradation of PFKFB3 protein expression (52).

The advent of high-throughput ''omics'' approaches, including epigenomics, transcriptomics, miRnomics, proteomics, and metabolomics (48), has provided a new mechanotransduction strategy to discover biomarkers with therapeutic targets. Jo and colleagues investigated the disturbed flow-mediated metabolites by using the blood plasma samples from ApoE$^{-/-}$ mice, and they demonstrated that 128 metabolites were significantly altered, including sphogomyelin, a common mammalian cell membrane sphingolipid in association with atherosclerosis (20). Our findings further support that flow-mediated VEGFR-PKCε-PFKFB3 signaling increases endothelial glycolytic metabolites for vascular regeneration. In addition, PKCε over-expression promotes glycolytic metabolites for myocardio-protection. Taken together, we elucidated a mechano-metabolomic pathway to promote DHA as a potential biomarker for vascular therapeutics.

Materials and Methods

Ethics statement

All animal experiments were performed in compliance with the University of California, Los Angeles (UCLA) Institutional Animal Care and Use Committee (IACUC) protocols, under a project license also approved by the UCLA IACUC. Humane care and use of animals were observed to minimize distress and discomfort.

Vascular endothelial cell culture

HAEC were purchased from Cell Applications and cultured in endothelial growth medium (Cell Applications) that was supplemented with 5% fetal bovine serum (FBS; Gibco). HAEC were propagated for experiments between passages 5 and 10.

siRNA transfection

siRNA transfection was performed with Lipofectamine RNAiMax (Invitrogen). HAEC were plated in six-well plates or standard glass slides on the day before transfection. The cells were transfected with 50 n*M* PKCε or KDR siRNA (Qiagen). Transfection media were changed to normal growth media after 4 h of transfection. Cells were used for confirmation of gene knockdown or assay at 48 h after transfection.

Chemical reagents

Human recombinant VEGF was purchased from Fisher Scientific and dissolved in phosphate-buffered saline (PBS). Cediranib was purchased from SelleckChem and dissolved in dimethyl sulfoxide (DMSO).

PKCε activity assay

PKCε activity assay with the ADP-Glo Kinase assay kit (Promega) was performed to assess activity change of PKCε in response to PSS and OSS. A confluent monolayer of HAEC on glass slides were subjected to three flow conditions: (i) static, (ii) PSS, and (iii) OSS, as previously described (34). After flow exposure, HAEC underwent the kinase reaction by adding a mixture of kinase reaction buffer. After a short incubation, ADP-Glo™ reagent (Promega) was added to terminate the kinase reaction and to deplete residual ATPs in the lysates. Next, a mixture of kinase detection reagents was added to introduce luciferase and luciferin from newly synthesized ATP, converted from ADP. The specificity was achieved by using PKCε-specific peptide as substrate. Luciferase activities were measured by using the Glo-Max Luminometer (Promega) as a readout of PKCε activity.

Quantitative real-time polymerase chain reaction analysis

PKCε and PFKFB3 mRNA expression was measured by quantitative RT-polymerase chain reaction (PCR). Total RNA was isolated by using Aurum Total RNA Mini Kit (Bio-Rad Laboratory). RNA was reverse transcribed by using iScript complementary DNA (cDNA) synthesis kit (Bio-Rad Laboratory), followed by PCR amplification with iScript RT-PCR Kit with SYBR Green (Bio-Rad Laboratory). The expression levels were normalized to actin.

The forward primer sequence for PKCε was 5′-GAG CCG CCA CTT CGA GGA CTG-3′, and the reverse primer was 5′-TTG TGG CCG TTG ACC TGA TGG-3′. The forward primer sequence for Actin was 5′-ACC CAC ACT GTG CCC ATC TAC-3′, and the reverse primer was 5′-TCG GTG AGG ATC TTC ATG AGG-3′. The forward primer sequence for PFKFB3 was 5′-GGA GGC TGT GAA GCA GTA CA-3′, and the

reverse primer was 5′-CAG CTA AGG CAC ATT GCT TC-3′. The differences in C_T values for various intervals *versus* control were used to determine the relative difference in the levels of PKCε mRNA expression.

SeaHorse mitochondrial function analysis

HAEC were infected with either CA-PKCε recombinant adenovirus (Adv-CA-PKCε) or DN-PKCε recombinant adenovirus (Adv-DN-PKCε), followed by treatment with or without 50 μM H_2O_2 in Dulbecco's modified Eagle's medium (DMEM) +1% FBS. Mitochondrial function was analyzed by using the Seahorse XF analyzer system as described with a 24-well assay plate format (50). Twenty thousand cells were loaded to individual wells of the 24-well SeaHorse analysis plate. Glycolysis levels were determined through measurements of the ECAR (53). Basal glycolysis was measured without treatment and maximum glycolysis was determined by treatment of the cells with 4 μM carbonyl cyanide p-trifluoromethoxy-phenylhydrazone (FCCP), the mitochondrial uncoupler, after basal measurement.

Dynamic flow system to assess vascular endothelial metabolites

A dynamic flow system was used to simulate well-defined PSS and OSS as previously described (34). The flow system was designed to generate physiologic shear stress occurring at human arterial branching points with well-defined slew rates, time-averaged shear stress, frequency, and amplitude. Confluent monolayers of HAEC grown on glass slides were subjected to three flow conditions at 1 Hz for 4 h: (i) static control at no flow state, (ii) pulsatile flow with time-averaged shear stress of 23 dyne·cm^{-2} accompanied by a stress slew rate ($\partial\tau/\partial t = 71$ dyne cm^{-2} s^{-1}), and (iii) oscillating flow (0.1 ± 4 dyne·cm^{-2}). ECs were maintained in DMEM culture media supplemented with 1% FBS at a temperature of 37°C and pH of 7.4 during flow exposure.

Endothelial metabolomic analysis

Metabolite samples were collected from HAEC treated with PSS ($\tau_{ave} = 50$ dyne·cm^{-2} accompanied by $\partial\tau/\partial t = 71$ dyne·cm^{-2}·s^{-1} at 1 Hz), OSS (0 ± 3 dyne·cm^{-2} with $\tau_{ave} = 0$ dyne·cm^{-2} at 1 Hz), or static conditions for 4 h (Supplementary Fig. S7). For oscillating flow, minimal forward flow at a mean shear stress of 0.2 dyne·cm^{-2} was provided every hour to deliver nutrients and to remove waste products. Cells were trypsinized, fixed in 4% paraformaldehyde (PFA), and immediately stored at −80°C before shipment in dry ice to the West Coast Metabolomics Center at UC Davis. GC-TOF analysis was performed to identify 156 known metabolites and 290 unknown compounds (18). Metabolites were reported with retention index, quantification mass, and full mass spectra. Quantification was by peak height without internal standards for absolute concentration.

PCA to assess significant metabolite change

PCAs were carried out by using the programming language R, version 2.14.0. Built-in ''ade4'' package was utilized to plot factorial maps with representation-of-point classes, which are denoted as Static, PSS, and OSS. Before performing PCAs, the concentrations of subjected metabolites were normalized by using the Pareto scaling method to put the measurements of different metabolites on the close scale. The *x*-axis in the figures was depicted as the first principal component (PC1) representing the space with the largest variance in data, whereas the *y*-axis was depicted as the second principal component (PC2) representing the space with the second largest variance. The ovals are 95% inertia ellipses.

Immunohistochemistry

Vascular rings corresponding to the aortic arch and thoracic aorta were cut from rabbit aorta segments, and they were immersed in 4% PFA. They were embedded in paraffin and cut into serial 5-μm sections. Immunostaining was performed with standard techniques in paraffin-embedded vascular tissue. Hematoxylin and eosin staining was used to observe gross vascular morphology, and PKCε and PFKFB3 staining was performed by using mouse monoclonal (PKCε, ABCAM) and goat polyclonal (PFKFB3, SCBT) antibodies. Tissue sections were viewed with a microscope, and images were captured with a CCD digital camera. Quantification of staining intensity was performed by using ImageJ software.

Tube formation assay

HAEC cells were grown in a 96-well plate at 20,000 cells/well on a 100 μl Matrigel growth-factor-reduced matrix (BD Biosciences) that was allowed to solidify before seeding cells in DMEM +5% FBS +25 ng/ml VEGF. Tube growth was allowed for 6 h, and wells were imaged to visualize tube formation with a microscope (Olympus). Images were analyzed by using S.CORE image analysis, with tube formation index representing a quantification of the images.

Transgenic Tg(flk-1:EGFP) *zebrafish model to study vascular injury and repair*

Tg(flk-1:EGFP) transgenic zebrafish embryos were generously provided by Prof. Ellen C. Lien (Children's Hospital Los Angeles, Los Angeles, CA) for assessing vascular injury and repair in response to tail amputation. *Flk-1*, VEGFR1, is tissue specific for vascular ECs. Fish embryos were injected with either a PKCε MO or a control nonsense MO. Injection was validated by qRT-PCR analysis of PKCε gene expression. The following MO sequences were used. Standard control negative MO: 5′-CCT CTT ACC TCA GTT ACA ATT TAT A-3′; zebrafish *p53* apoptosis suppression MO (p53MO): 5′-GCG CCA TTG CTT TGC AAG AAT TG-3′; *PKC*ε splice MO: 5′-CTC CAT TAA AAA CCA CCA TGA TGA C-3′; *GATA-1a* MO: 5′-CTGCAAGTGTAGTATTGAAGATGTC-3′; *TNNT-2a* MO: (5′-CGCGTGGACAGATTCAAGAGCCCTC-3′. MOs were dissolved in water to make 0.3 mM stock solution with addition of 0.1 mM p53 MO. Immediately after collection at 0 hpf, approximately 30–40 embryos were randomly chosen for micro-injections. All the embryos were maintained in E3 medium at 28°C.

Injected fish larvae were grown to 72 hpf in standard E3 medium, followed by amputation of the posterior tail segment ~ 100 μm from the tip of the tail. The larvae were anesthetized in 0.02% tricaine solution to allow for precise placement. Amputation was performed with a surgical scalpel under a stereo microscope (MEIJI Techno EMZ series;

MEIJI) for both control and treatment groups. After amputation, fish were separated to allow for same-fish control. Fish tail sections were imaged (Olympus IX71; Olympus) to visualize the blood vessels immediately after amputation and every 24 h thereafter over the next 3 days. Regeneration of blood vessels was compared between the different treatment groups at 0, 1, and 3 dpa.

Cloning of PKCε mRNA for rescue

Mouse PKCε cDNA was amplified from a donor plasmid (Addgene) and cloned into the plasmid pCS2+ at the *Bam*HI and *Eco*RI sites. Clones with the PKCε cDNA insert were selected by PCR screening. The pCS2+PKCε plasmid was verified by transfecting the plasmids into HEK-293 cells, followed by detecting PKCε protein expression by Western blot with anti-PKCε antibody. mRNA was synthesized from the cloned plasmid by using the mMessage SP6 kit (Invitrogen). Transcribed PKCε mRNA was purified with the total RNA isolation kit (Bio-Rad Laboratory) for *in vivo* rescue experiments.

Blood shear stress modulation

Shear stress (τ) is characterized as dynamic viscosity (μ) of fluid multiplied by shear rate ($\dot{\gamma}$), defined as a gradient of velocity between two adjacent fluid layers (32):

$$\tau = \mu \cdot \dot{\gamma} = \mu \frac{\partial u_x}{\partial_y} \quad (1)$$

where $\frac{\partial u_x}{\partial y}$ is the tangential velocity gradient between two adjacent fluid layers. Since shear stress is a function of viscosity (μ), injection of *GATA-1a* MO to inhibit erythrocytosis reduced viscosity, whereas injection of *EPO* mRNA resulted in the opposite effects to the endothelium (Supplementary Videos S1–S3).

Western blot analysis

Cells were harvested, washed with PBS, and lysed with RIPA buffer. The lysate was centrifuged at 12,000 *g* for 10 min, and the resulting supernatants were used as the entire cell lysate. Proteins were separated by 4–20% polyacrylamide gel with sodium dodecyl sulfate (SDS), electroblotted onto the polyvinylidene difluoride membranes (GE Healthcare), and blocked overnight at 4°C in Tris buffered saline-Tween20 (TBS-T) containing 5% non-fat dry milk (Bio-Rad Laboratory). PKCε protein expression was detected with anti-PKCε (Santa Cruz Biotech), and equal loading was verified by blotting with anti-β-tubulin (Millipore, Inc.). After treatment with peroxidase-conjugated anti-goat (Santa Cruz Biotech) or anti-mouse IgG antibody (Jackson ImmunoResearch) for 1 h at room temperature, chemilluminescence signal was developed with Supersignal Western Pico (Pierce) and recorded with FluorChem FC2 (Alpha Inotech, Inc.). Antibodies against autophagy-associated genes were purchased from Boster Biological Technologies for p62. Parallel blots were performed with anti-β-tubulin (Millipore, Inc.) for loading normalization. Densitometry was performed to quantify blot bands as previously described (34).

Mitochondrial superoxide assay

Mitochondrial superoxide ($mtO_2^{\bullet-}$) was analyzed both quantitatively by flow cytometry and qualitatively by fluorescent imaging as previously described (34). Briefly, in a six-well format for FACS analysis, cells were incubated with 10 μM mitoSOX dye (Invitrogen) for 15 min, then lysed, and finally rinsed three times with PBS buffer to remove residual dye. Samples were then analyzed by using FACS analysis, with gating to remove debris or clusters.

For qualitative imaging of $mtO_2^{\bullet-}$ levels during tube formation, tube formation assay was performed, as described earlier, with media that were absent of phenol red. At 6 h, cells were incubated with 10 μM mitoSOX dye for 30 min, rinsed three times with Dulbecco's PBS, and finally fixed with PFA. Cells were imaged by using fluorescent microscopy.

Statistical analysis

Data were expressed as mean ± standard error of the mean unless otherwise stated. Multiple comparisons were performed by one-way analysis of variance, and statistical significance for comparison between two groups was determined by student *t*-test, two-sample proportional z-test, or Wilcoxon rank-sum test (non-parametric analysis) when data were not normally distributed. A p-value <0.05 was considered statistically significant.

Acknowledgments

The authors would like to express their gratitude to Dr. Manuel Mayr for providing the metabolomic analysis of PKCε-mediated cardiac metabolites. Human CA-PKCε and dominant-negative PKCε adenoviruses were generously provided by Dr. Allen Samarel at the Loyola University Medical Center. This study was supported by the National Institutes of Health HL118650, HL083015, and HL129727 (T.K.H.).

Author Disclosure Statement

No competing financial interests exist.

References

1. Parkinson disease. Metablomics study reveals novel biomarkers for PD. *Nat Rev Neurol* 9: 484, 2013.
2. Stroke. Molecular markers could help predict stroke risk after TIA. *Nat Rev Neurol* 11: 3, 2015.
3. Bakker JL, Meijers-Heijboer H, and Verheul H. Novel strategies towards the use of anti-angiogenic agents in breast cancer. *Eur J Pharmacol* 717: 36–39, 2013.
4. Boo YC, Sorescu G, Boyd N, Shiojima I, Walsh K, Du J, and Jo H. Shear stress stimulates phosphorylation of endothelial nitric-oxide synthase at Ser1179 by Akt-independent mechanisms: Role of protein kinase A. *J Biol Chem* 277: 3388–3396, 2002.
5. Boselli F, Freund JB, and Vermot J. Blood flow mechanics in cardiovascular development. *Cell Mol Life Sci* 72: 2545–2559, 2015.
6. Budas G, Costa HM, Jr, Ferreira JC, Teixeira da Silva Ferreira A, Perales J, Krieger JE, Mochly-Rosen D, and Schechtman D. Identification of epsilonPKC targets during cardiac ischemic injury. *Circ J* 76: 1476–1485, 2012.
7. Cao H, Yu F, Zhao Y, Scianmarello N, Lee J, Dai W, Jen N, Beebe T, Li R, Ebrahimi R, Chang DS, Mody FV,

Pacella J, Tai YC, and Hsiai T. Stretchable electrochemical impedance sensors for intravascular detection of lipid-rich lesions in New Zealand White rabbits. *Biosens Bioelectron* 54: 610–616, 2014.
8. Chiu JJ, Wang DL, Chien S, Skalak R, and Usami S. Effects of disturbed flow on endothelial cells. *J Biomech Eng* 120: 2–8, 1998.
9. Chu CY, Cheng CH, Chen GD, Chen YC, Hung CC, Huang KY, and Huang CJ. The zebrafish erythropoietin: Functional identification and biochemical characterization. *FEBS Lett* 581: 4265–4271, 2007.
10. Clyne M. Kidney cancer: Metabolomics for targeted therapy. *Nat Rev Urol* 9: 355, 2012.
11. Culic O, Gruwel ML, and Schrader J. Energy turnover of vascular endothelial cells. *Am J Physiol* 273: C205–C213, 1997.
12. De Bock K, Georgiadou M, and Carmeliet P. Role of endothelial cell metabolism in vessel sprouting. *Cell Metab* 18: 634–647, 2013.
13. De Bock K, Georgiadou M, Schoors S, Kuchnio A, Wong BW, Cantelmo AR, Quaegebeur A, Ghesquiere B, Cauwenberghs S, Eelen G, Phng LK, Betz I, Tembuyser B, Brepoels K, Welti J, Geudens I, Segura I, Cruys B, Bifari F, Decimo I, Blanco R, Wyns S, Vangindertael J, Rocha S, Collins RT, Munck S, Daelemans D, Imamura H, Devlieger R, Rider M, Van Veldhoven PP, Schuit F, Bartrons R, Hofkens J, Fraisl P, Telang S, Deberardinis RJ, Schoonjans L, Vinckier S, Chesney J, Gerhardt H, Dewerchin M, and Carmeliet P. Role of PFKFB3-driven glycolysis in vessel sprouting. *Cell* 154: 651–663, 2013.
14. Dejana E. The role of wnt signaling in physiological and pathological angiogenesis. *Circ Res* 107: 943–952, 2010.
15. Doddaballapur A, Michalik KM, Manavski Y, Lucas T, Houtkooper RH, You X, Chen W, Zeiher AM, Potente M, Dimmeler S, and Boon RA. Laminar shear stress inhibits endothelial cell metabolism via KLF2-mediated repression of PFKFB3. *Arterioscler Thromb Vasc Biol* 35: 137–145, 2015.
16. Dorn GW, 2nd, and Mochly-Rosen D. Intracellular transport mechanisms of signal transducers. *Annu Rev Physiol* 64: 407–429, 2002.
17. Dunn J, Qiu H, Kim S, Jjingo D, Hoffman R, Kim CW, Jang I, Son DJ, Kim D, Pan C, Fan Y, Jordan IK, and Jo H. Flow-dependent epigenetic DNA methylation regulates endothelial gene expression and atherosclerosis. *J Clin Invest* 124: 3187–3199, 2014.
18. Fiehn O, Wohlgemuth G, Scholz M, Kind T, Lee do Y, Lu Y, Moon S, and Nikolau B. Quality control for plant metabolomics: Reporting MSI-compliant studies. *Plant J* 53: 691–704, 2008.
19. Frangos JA, McIntire LV, and Eskin SG. Shear stress induced stimulation of mammalian cell metabolism. *Biotechnol Bioeng* 32: 1053–1060, 1988.
20. Go YM, Kim CW, Walker DI, Kang DW, Kumar S, Orr M, Uppal K, Quyyumi AA, Jo H, and Jones DP. Disturbed flow induces systemic changes in metabolites in mouse plasma: A metabolomics study using ApoE(-)/(-) mice with partial carotid ligation. *Am J Physiol Regul Integr Comp Physiol* 308: R62–R72, 2015.
21. Guo D, Chien S, and Shyy JY. Regulation of endothelial cell cycle by laminar versus oscillatory flow: Distinct modes of interactions of AMP-activated protein kinase and Akt pathways. *Circ Res* 100: 564–571, 2007.
22. Hwang J, Ing MH, Salazar A, Lassegue B, Griendling K, Navab M, Sevanian A, and Hsiai TK. Pulsatile versus oscillatory shear stress regulates NADPH oxidase subunit expression: Implication for native LDL oxidation. *Circ Res* 93: 1225–1232, 2003.
23. Jalali S, Li YS, Sotoudeh M, Yuan S, Li S, Chien S, and Shyy JY. Shear stress activates p60src-Ras-MAPK signaling pathways in vascular endothelial cells. *Arterioscler Thromb Vasc Biol* 18: 227–234, 1998.
24. Jen N, Yu F, Lee J, Wasmund S, Dai X, Chen C, Chawareeyawong P, Yang Y, Li R, Hamdan MH, and Hsiai TK. Atrial fibrillation pacing decreases intravascular shear stress in a New Zealand white rabbit model: Implications in endothelial function. *Biomech Model Mechanobiol* 12: 735–745, 2013.
25. Jones R, Baker MB, Weber M, Harrison DG, Bao G, and Searles CD. Molecular beacons can assess changes in expression and 3′-polyadenylation of human eNOS mRNA. *Am J Physiol Cell Physiol* 296: C498–C504, 2009.
26. Kang M and Walker JW. Protein kinase C delta and epsilon mediate positive inotropy in adult ventricular myocytes. *J Mol Cell Cardiol* 38: 753–764, 2005.
27. Kluge MA, Fetterman JL, and Vita JA. Mitochondria and endothelial function. *Circ Res* 112: 1171–1188, 2013.
28. Koh W, Sachidanandam K, Stratman AN, Sacharidou A, Mayo AM, Murphy EA, Cheresh DA, and Davis GE. Formation of endothelial lumens requires a coordinated PKCepsilon-, Src-, Pak- and Raf-kinase-dependent signaling cascade downstream of Cdc42 activation. *J Cell Sci* 122: 1812–1822, 2009.
29. Kulkeaw K and Sugiyama D. Zebrafish erythropoiesis and the utility of fish as models of anemia. *Stem Cell Res Ther* 3: 55, 2012.
30. Kumar S and Hedges SB. A molecular timescale for vertebrate evolution. *Nature* 392: 917–920, 1998.
31. Lee J, Fei P, Sevag Packard RR, Kang H, Xu H, Baek KI, Jen N, Chen J, Yen H, Kuo CC, Chi NC, Ho CM, Li R, and Hsiai TK. 4-Dimensional light-sheet microscopy to elucidate shear stress modulation of cardiac trabeculation. *J Clin Invest* 126: 3158, 2016.
32. Lee J, Packard RR, and Hsiai TK. Blood flow modulation of vascular dynamics. *Curr Opin Lipidol* 26: 376–383, 2015.
33. Li R, Beebe T, Jen N, Yu F, Takabe W, Harrison M, Cao H, Lee J, Yang H, Han P, Wang K, Shimizu H, Chen J, Lien CL, Chi NC, and Hsiai TK. Shear stress-activated Wnt-angiopoietin-2 signaling recapitulates vascular repair in zebrafish embryos. *Arterioscler Thromb Vasc Biol* 34: 2268–2275, 2014.
34. Li R, Jen N, Wu L, Lee J, Fang K, Quigley K, Lee K, Wang S, Zhou B, Vergnes L, Chen YR, Li Z, Reue K, Ann DK, and Hsiai TK. Disturbed flow induces autophagy, but impairs autophagic flux to perturb mitochondrial homeostasis. *Antioxid Redox Signal* 23: 1207–1219, 2015.
35. Ma J, Luo Y, Sevag Packard RR, Ma T, Ding Y, Abiri P, Tai YC, Zhou Q, Shung KK, Li R, and Hsiai T. Ultrasonic transducer-guided electrochemical impedance spectroscopy to assess lipid-laden plaques. *Sens Actuators B Chem* 235: 154–161, 2016.
36. Mayr M, Liem D, Zhang J, Li X, Avliyakulov NK, Yang JI, Young G, Vondriska TM, Ladroue C, Madhu B, Griffiths JR, Gomes A, Xu Q, and Ping P. Proteomic and metabolomic analysis of cardioprotection: Interplay between

protein kinase C epsilon and delta in regulating glucose metabolism of murine hearts. *J Mol Cell Cardiol* 46: 268–277, 2009.
37. Milan DJ, Jones IL, Ellinor PT, and MacRae CA. In vivo recording of adult zebrafish electrocardiogram and assessment of drug-induced QT prolongation. *Am J Physiol Heart Circ Physiol* 291: H269–H273, 2006.
38. Morbiducci U, Kok AM, Kwak BR, Stone PH, Steinman DA, and Wentzel JJ. Atherosclerosis at arterial bifurcations: Evidence for the role of haemodynamics and geometry. *Thromb Haemost* 115: 484–492, 2016.
39. Neufer PD, Bamman MM, Muoio DM, Bouchard C, Cooper DM, Goodpaster BH, Booth FW, Kohrt WM, Gerszten RE, Mattson MP, Hepple RT, Kraus WE, Reid MB, Bodine SC, Jakicic JM, Fleg JL, Williams JP, Joseph L, Evans M, Maruvada P, Rodgers M, Roary M, Boyce AT, Drugan JK, Koenig JI, Ingraham RH, Krotoski D, Garcia-Cazarin M, McGowan JA, and Laughlin MR. Understanding the cellular and molecular mechanisms of physical activity-induced health benefits. *Cell Metab* 22: 4–11, 2015.
40. Novellasdemunt L, Tato I, Navarro-Sabate A, Ruiz-Meana M, Mendez-Lucas A, Perales JC, Garcia-Dorado D, Ventura F, Bartrons R, and Rosa JL. Akt-dependent activation of the heart 6-phosphofructo-2-kinase/fructose-2,6-bisphosphatase (PFKFB2) isoenzyme by amino acids. *J Biol Chem* 288: 10640–10651, 2013.
41. Packard RR, Zhang X, Luo Y, Ma T, Jen N, Ma J, Demer LL, Zhou Q, Sayre JW, Li R, Tai YC, and Hsiai TK. Two-point stretchable electrode array for endoluminal electrochemical impedance spectroscopy measurements of lipid-laden atherosclerotic plaques. *Ann Biomed Eng* 44: 2695–2706, 2016.
42. Painter RM, Pearson DM, and Waymouth RM. Selective catalytic oxidation of glycerol to dihydroxyacetone. *Angew Chem Int Ed Engl* 49: 9456–9459, 2010.
43. Prokopiou EM, Ryder SA, and Walsh JJ. Tumour vasculature targeting agents in hybrid/conjugate drugs. *Angiogenesis* 16: 503–524, 2013.
44. Rask-Madsen C and King GL. Differential regulation of VEGF signaling by PKC-alpha and PKC-epsilon in endothelial cells. *Arterioscler Thromb Vasc Biol* 28: 919–924, 2008.
45. Roman BL and Pekkan K. Mechanotransduction in embryonic vascular development. *Biomech Model Mechanobiol* 11: 1149–1168, 2012.
46. Schoors S, De Bock K, Cantelmo AR, Georgiadou M, Ghesquiere B, Cauwenberghs S, Kuchnio A, Wong BW, Quaegebeur A, Goveia J, Bifari F, Wang X, Blanco R, Tembuyser B, Cornelissen I, Bouche A, Vinckier S, Diaz-Moralli S, Gerhardt H, Telang S, Cascante M, Chesney J, Dewerchin M, and Carmeliet P. Partial and transient reduction of glycolysis by PFKFB3 blockade reduces pathological angiogenesis. *Cell Metab* 19: 37–48, 2014.
47. Sedmera D, Reckova M, deAlmeida A, Sedmerova M, Biermann M, Volejnik J, Sarre A, Raddatz E, McCarthy RA, Gourdie RG, and Thompson RP. Functional and morphological evidence for a ventricular conduction system in zebrafish and Xenopus hearts. *Am J Physiol Heart Circ Physiol* 284: H1152–H1160, 2003.
48. Simmons RD, Kumar S, and Jo H. The role of endothelial mechanosensitive genes in atherosclerosis and omics approaches. *Arch Biochem Biophys* 591: 111–131, 2016.
49. Suarez J and Rubio R. Regulation of glycolytic flux by coronary flow in guinea pig heart. Role of vascular endothelial cell glycocalyx. *Am J Physiol* 261: H1994–H2000, 1991.
50. Subramaniam SR, Vergnes L, Franich NR, Reue K, and Chesselet M-F. Region specific mitochondrial impairment in mice with widespread overexpression of alpha-synuclein. *Neurobiol Dis* 70: 204–213, 2014.
51. Sun X and Feinberg MW. Regulation of endothelial cell metabolism: Just go with the flow. *Arterioscler Thromb Vasc Biol* 35: 13–15, 2015.
52. Takabe W, Li R, Ai L, Yu F, Berliner JA, and Hsiai TK. Oxidized low-density lipoprotein-activated c-Jun NH2-terminal kinase regulates manganese superoxide dismutase ubiquitination: Implication for mitochondrial redox status and apoptosis. *Arterioscler Thromb Vasc Biol* 30: 436–441, 2010.
53. TeSlaa T and Teitell MA. Techniques to monitor glycolysis. *Methods Enzymol* 542: 91–114, 2014.
54. Wang S, Iring A, Strilic B, Albarran Juarez J, Kaur H, Troidl K, Tonack S, Burbiel JC, Muller CE, Fleming I, Lundberg JO, Wettschureck N, and Offermanns S. P2Y2 and Gq/G11 control blood pressure by mediating endothelial mechanotransduction. *J Clin Invest* 125: 3077–3086, 2015.
55. Wang Y and Ashraf M. Role of protein kinase C in mitochondrial KATP channel-mediated protection against Ca^{2+} overload injury in rat myocardium. *Circ Res* 84: 1156–1165, 1999.
56. Wang Y, Zang QS, Liu Z, Wu Q, Maass D, Dulan G, Shaul PW, Melito L, Frantz DE, Kilgore JA, Williams NS, Terada LS, and Nwariaku FE. Regulation of VEGF-induced endothelial cell migration by mitochondrial reactive oxygen species. *Am J Physiol Cell Physiol* 301: C695–C704, 2011.
57. Wu M, Neilson A, Swift AL, Moran R, Tamagnine J, Parslow D, Armistead S, Lemire K, Orrell J, Teich J, Chomicz S, and Ferrick DA. Multiparameter metabolic analysis reveals a close link between attenuated mitochondrial bioenergetic function and enhanced glycolysis dependency in human tumor cells. *Am J Physiol Cell Physiol* 292: C125–C136, 2007.
58. Yu F, Lee J, Jen N, Li X, Zhang Q, Tang R, Zhou Q, Kim ES, and Hsiai TK. Elevated electrochemical impedance in the endoluminal regions with high shear stress: Implication for assessing lipid-rich atherosclerotic lesions. *Biosens Bioelectron* 43: 237–244, 2013.

Address correspondence to:
Prof. Tzung K. Hsiai
Division of Cardiology
Department of Medicine
University of California, Los Angeles
10833 Le Conte Avenue, CHS17-054A
Los Angeles, CA 90095-1679

Department of Bioengineering
University of California, Los Angeles
10833 Le Conte Avenue, CHS17-054A
Los Angeles, CA 90095-1679

E-mail: thsiai@mednet.ucla.edu

Date of first submission to ARS Central, March 8, 2017; date of final revised submission, July 31, 2017; date of acceptance, July 31, 2017.

Abbreviations Used

CA = constitutively active
cDNA = complementary DNA
DHA = dihydroxyacetone
DMEM = Dulbecco's modified Eagle's medium
DN = dominant negative
dpa = days post-amputation
EC = endothelial cell
ECAR = extracellular acidification rates
eNOS = endothelial nitric oxide synthase
EPO = erythropoietin
FBS = fetal bovine serum
GC-TOF = gas chromatography time-of-flight mass spectrometry
HAEC = human aortic endothelial cells
hpf = hours post-fertilization
IACUC = Institutional Animal Care and Use Committee
I/R = ischemia/reperfusion
KLF2 = Krüppel-like factor 2
LSS = laminar shear stress
MO = morpholino oligonucleotide
mRNA = messenger RNA
$mtO_2^{\bullet-}$ = mitochondrial superoxide
NZW = New Zealand White
OSS = oscillatory shear stress
PBS = phosphate-buffered saline
PCA = principal component analysis
PCR = polymerase chain reaction
PFA = paraformaldehyde
PFKFB3 = 6-phosphofructo-2-kinase/fructose-2, 6-biphosphatase 3
PKCε = protein kinase C isoform epsilon
PSS = pulsatile shear stress
ROS = reactive oxygen species
Scr = scrambled
siRNA = small interfering RNA
UCLA = University of California, Los Angeles
VEGFR = vascular endothelial growth factor receptor